International Journal of Heat and Mass Transfer 52 (2009) 2932–2941

Contents lists available at ScienceDirect

International Journal of Heat and Mass Transfer

journal homepage: www.elsevier.com/locate/ijhmt

Chaotic behavior of pulsating heat pipes

Yanxi Song, Jinliang Xu *

Micro Energy System Laboratory, Guangzhou Institute of Energy Conversion, Chinese Academy of Science, Guangzhou 510640, PR China

ARTICLE INFO

Article history:
Received 28 August 2008
Received in revised form 16 February 2009
Accepted 17 February 2009
Available online 5 April 2009

Keywords:
Pulsating heat pipe
Nonlinear analysis
Correlation dimension
Kolmogorov entropy

ABSTRACT

Chaotic behavior of closed loop pulsating heat pipes (PHPs) was studied. The PHPs were fabricated by capillary tubes with outer and inner diameters of 2.0 and 1.20 mm. FC-72 and deionized water were used as the working fluids. Experiments cover the following data ranges: number of turns of 4, 6, and 9, inclination angles from 5° (near horizontal) to 90° (vertical), charge ratios from 50% to 80%, heating powers from 7.5 to 60.0 W. The nonlinear analysis is based on the recorded time series of temperatures on the evaporation, adiabatic, and condensation sections. The present study confirms that PHPs are deterministic chaotic systems. Autocorrelation functions (ACF) are decreased versus time, indicating prediction ability of the system is finite. Three typical attractor patterns are identified. Hurst exponents are very high, i.e., from 0.85 to 0.95, indicating very strong persistent properties of PHPs. Curves of correlation integral versus radius of hypersphere indicate two linear sections for water PHPs, corresponding to both high frequency, low amplitude, and low frequency, large amplitude oscillations. At small inclination angles near horizontal, correlation dimensions are not uniform at different turns of PHPs. The non-uniformity of correlation dimensions is significantly improved with increases in inclination angles. Effect of inclination angles on the chaotic parameters is complex for FC-72 PHPs, but it is certain that correlation dimensions and Kolmogorov entropies are increased with increases in inclination angles. The optimal charge ratios are about 60–70%, at which correlation dimensions and Kolmogorov entropies are high. The higher the heating power, the larger the correlation dimensions and Kolmogorov entropies are. For most runs, large correlation dimensions and Kolmogorov entropies correspond to small thermal resistances, i.e., better thermal performance, except for FC-72 PHPs at small inclination angles of $\theta < 15°$.

1. Introduction

In the 1990s, Akachi et al. [1] proposed a new type of heat pipe known as the *pulsating* or *oscillating heat pipe* (PHP or OHP). As a passive heat transfer device, PHP has potential applications in electronic cooling because it may dissipate high heat fluxes created by the next generation electronics. PHPs differ from conventional heat pipes in several major ways. A PHP is a snake-shaped capillary tube that is partially filled with liquid. As seen in Fig. 1, the tube is bent back and forth parallel to itself, and the ends of the tube may be connected to one another in a closed loop, or pinched off and welded shut in an open loop [2].

Once the inside diameter of the capillary tube satisfies the criterion of $d < d_{cr} = 2[\sigma/g(\rho_f - \rho_g)]^{0.5}$, partially filled liquid in capillaries involves segmented liquid slugs and vapor plugs. When heating is applied on the evaporation section, pressures in parallel capillary channels may be different due to the non-uniform lengths of vapor plugs and liquid slugs, causing fluid movement in capillaries. The fluid movement changes the initial distribution of vapor and liquid phases, causing the change of pressure distribution in parallel channels, leading to fluid transport in the direction that is inverse to the initial fluid movement. Continuous heating sustains the oscillation flow. When the fluid is transported from the evaporation section to the condensation section, heat is transferred from the higher temperature zone to the lower temperature zone. Maezawa et al. [3] observed in their experimental work that, at a specific condition, dry-out occurred and the closed loop PHP failed to work.

Phenomenon in a PHP is very complicated. A recent paper by Zhang and Faghri [2] gave a review on the working principle, research and development, effects of various parameters such as working fluids, charge ratios, inclination angles, etc. on the fluid dynamics and heat transfer. Available studies on PHPs can be categorized as either experimental or theoretical. Experimental investigations focused on either the visualization of flow patterns or characterizing the thermal performance of PHPs. Theoretical works attempt to analytically or numerically compute the fluid dynamics and/or heat transfer associated with the oscillating two-phase flow.

Zhang and Faghri [4] modeled heat transfer in the evaporator and condenser sections of a PHP with open end by analyzing thin film evaporation and condensation. The heat transfer solutions are applied to the thermal model of the PHP and a parametric

* Corresponding author. Tel.: +86 20 87057656.
E-mail address: xujl@ms.giec.ac.cn (J. Xu).

0017-9310/$ - see front matter © 2009 Elsevier Ltd. All rights reserved.
doi:10.1016/j.ijheatmasstransfer.2009.02.030

Nomenclature

AC	autocorrelation function coefficient
$B(t,u)$	average departure to average value of time series of T
$C(r)$	correlation integral
D_2	correlation dimension
d	inside diameter of capillary tube (m)
d_{cr}	critical inner diameter of capillary tube (m)
g	gravity acceleration (m/s^2)
H	heaviside function
H_{fg}	latent heat of evaporation (J/kg)
k	constant in Eq. (6)
l_c	specific distance with a pair of vectors
m	embedded dimension
N	number of data points
Q	heating power (W)
q	heat flux (W/m^2)
R	thermal resistance (°C/W)
r	radius of a hypersphere
$S(t,\tau)$	standard deviation
T	temperature (°C)
T_{sat}	saturation temperature (°C)
$\langle T\rangle$	average temperature (°C)
t	time (s)
u	integration index
$\mathbf{X}$	vector time series
α	charge ratio
ρ_f, ρ_g	liquid and vapor density (kg/m^3)
σ	surface tension force (N/m)
θ	inclination angle
τ	delay time (s)
Δt	sampling interval (s)
ΔT_{max}	maximum temperature difference in the temperature series in 10 min (°C)

study was performed. The results show that the heat transfer is mainly due to the exchange of sensible heat. The oscillation frequency and amplitude is almost unaffected by surface tension after steady oscillation is established.

Holley and Faghri [5] proposed a one-dimensional model with slug flow where the momentum equation was solved. The energy equation is solved in the wall, wick, and working fluids. Results show that heat transfer capability can be increased using the varied cross section of the channel.

Khandekar et al. [6] experimentally studied PHPs using water and ethanol as working fluids. They found that PHP does not work at horizontal orientation but operated vertically as a thermosyphon. Performance depends on orientation, charge ratio, and cross-section geometry.

Khandekar et al. [7] discussed important issues involved in the mathematical modeling of PHPs. Semi-empirical correlations based on non-dimensional numbers of interest for predicting the thermal performance of closed loop PHPs were presented. Although there are limitations of the models presented, modeling by non-dimensional numbers seems to be most promising as compared to other existing techniques.

Dobson [8] simulated open loop PHPs taking gravity, surface tension, friction, and pressure into account. The model used vapor bubble, liquid plug, and liquid film as control volumes. The model was able to predict the experimentally determined values. It was recommended that convective heat transfer is further studied and the water pumping ability is exploited.

Tong et al. [9] performed flow visualization for the closed loop PHP. It was observed that during the start-up period, the working fluid oscillates with large amplitude, however, at steady operating state, the working fluid circulates. Phenomena such as nucleation boiling, coalescence of bubbles, formation of slug, and propagation of inertia wave were observed in the closed loop PHP. The findings showed that the meandering bends, uneven slug and plug distribution, and non-concurrent boiling at the evaporator contributed to the driving and restoring forces for fluid circulation and oscillations.

Lin et al. [10] studied PHPs using FC-72 and FC-75 as the working fluids. It is found that the evaporator was dried out when charge ratios were less than 40%. At a charge ratio of 50%, the PHP could dissipate 2040 W of heat. They concluded that PHP performance was independent of orientation using the two working fluids.

Cai et al. [11] presented an experimental investigation of heat transfer characteristics of PHPs versus operating temperatures. The PHP with 12 turns was made of stainless steel or copper and charged with water at three charge ratios: 40%, 55%, and 70%. They found that minimum temperature difference and fluctuation appear at temperatures between 120 and 160 °C.

Ma et al. [12] performed an experimental investigation of a nanofluid oscillating heat pipe (OHP) to determine the nanofluid effect on the heat transport capability in an OHP. The nano particles filled in the OHP had the volume concentration of 1.0% with the particle size in the range of 5–50 nm. Experimental results show that the heat transport capability of the OHP significantly increased when it was charged with the nanofluid at a charge ratio of 50%. The heat transport capability of the OHP depends on the operating temperature. The investigated OHP could reach a thermal resistance of 0.03 °C/W at a heat input of 336 W.

Recently, Xu et al. [13] performed flow visualizations of PHPs. It is found that there exists bulk circulation flow and local flow direction switch flow. Methanol PHPs display the sine oscillation waves but water PHPs show the quasi rectangular shape for the bubble displacements and velocities, accounted by larger latent heat of evaporation.

The above reviews show that experimental studies are focused on characterizing the thermal performance, while numerical/theoretical works are based on the deterministic point of view. As noted by Zhang and Faghri [2], there are many issues unsolved at this stage. The objective of this paper is to verify that PHPs are deterministic chaotic systems, using the nonlinear analysis method. The analysis is based on the recorded time series of temperatures on the evaporation, adiabatic, and condensation sections. Because there are many factors influencing the PHP performance, effects of these parameters on the complexity of PHPs were examined one by one. The present study establishes a relationship of chaotic parameters (correlation dimensions and Kolmogorov entropies) with PHP thermal performance, providing design and operation guidelines for pulsating heat pipes. It is noted that nonlinear analysis of PHPs is less reported in the literature.

2. Experimental setup

The experimental setup, as shown in Fig. 1, consists of a power supply unit, three selective PHP units, and a high speed data acquisition system. The power supply unit includes an AC voltage stabi-

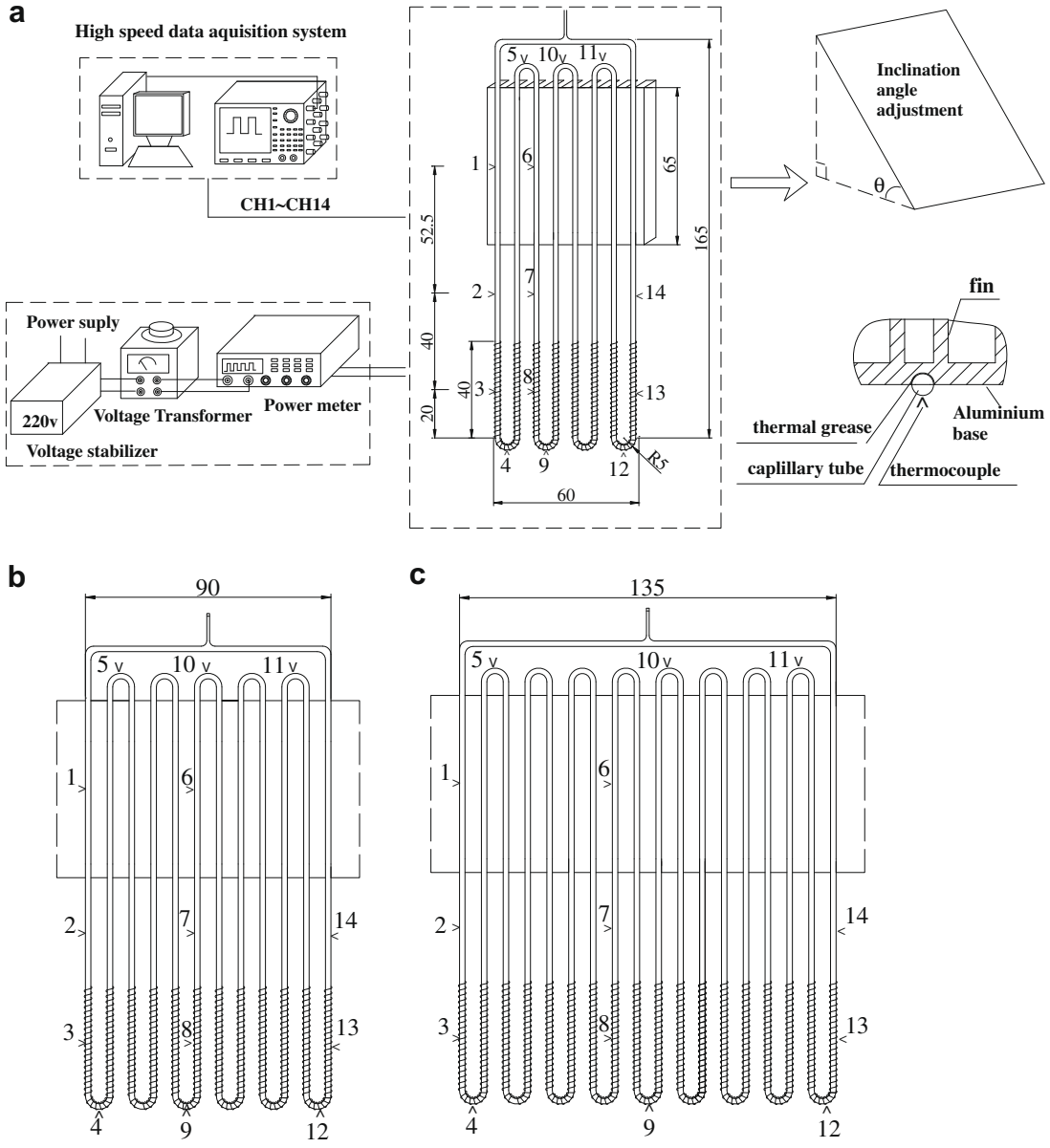

Fig. 1. Experimental setup for PHPs, (a) four turns, (b) six turns, and (c) nine turns.

lizer, a voltage transformer, and a power meter. Adjusting the voltage transformer yields a stable voltage output in the range of 2–220 V, corresponding to a controllable power of 1–200 W. The power meter measures the voltage, current, and power simultaneously applied on the evaporation section. The maximum uncertainty of the power reading is 1.0%.

A high speed data acquisition system (DL750, Yokogawa, Inc., Japan) was used to record time series of temperatures at different locations on the PHPs. The data sampling rate can be up to 100 K samples per second. In the present study, we used the sampling rate of 20/s, which is at least one order higher than the characteristic frequencies of temperature oscillations of PHPs. For each run, the physical recording time is 600 s. Thus, there were 12,000 data points for each temperature signal and 168,000 data points for the 14 temperature signals.

In order to identify effect of number of turns of the capillary tube on the PHP thermal performance, three PHPs were used, which are shown in Fig. 1a for four turns, b for six turns, and c for nine turns. The PHP was positioned on a specific designed test rig, which adjusts the inclination angle from exact horizontal plane ($\theta = 0^\circ$) to vertical plane ($\theta = 90^\circ$). The angle uncertainty is 1°. All three PHPs were fabricated using a long copper capillary tube with an outer diameter of 2.0 mm and an inner diameter of 1.20 mm. The bending radius was 5 mm. Based on the criterion of the inside diameter of capillary tube for the formation of vapor plugs and liquid slugs in the capillary tube, the critical diameter is 1.46 mm for FC-72. The present study uses the diameter of 1.2 mm, satisfying the critical size criterion. Therefore, the mixture of vapor plug and liquid slug can be formed in the capillary tube. The detected temperature oscillation on the capillary wall surface is a direct evidence of the pulsating flow caused by the vapor plug and liquid slug pattern under the heating condition. A heating (evaporation), an adiabatic, and a cooling (condensation) section were included in PHPs. In the evaporation section, the thermal load was applied by wrapping the Ni–Cr metallic wire with a diameter of 0.4 mm (12 Ω/m) on the outer surface

of the capillary tube. An aluminum fin heat sink was adapted on the top part of the PHP, forming the condensation section. The fin height was 8.0 mm and thickness was 2.0 mm. The gap distance between neighboring fins was 4.0 mm. The copper capillary tube was embedded on the base surface of the aluminum fin heat sink (see Fig. 1a). Thermal grease was filled between the fin heat sink and the capillary tube to lower the conduction thermal resistance. Aluminum fin heat sinks were also adapted with the six and nine turns PHPs. The dashed rectangular area is the projected area for the fin heat sink (see Fig. 1b and c). Forced convective air was supplied by a centrifugal fan to dissipate heat received by the aluminum heat sink. The fan was driven by a 12 V DC power supply and the operation condition keeps the same for all the tests in this study. Below the fin heat sink, the capillary tube was well-insulated.

All the three PHPs had a total height of 165 mm. The evaporation, adiabatic, and condensation sections had lengths of 40, 40, and 65 mm, respectively. The four, six, and nine turns of PHPs had widths of 60, 90, and 135 mm, respectively (see Fig. 1a–c). For each PHP assembly, the fin heat sink was wider than the PHP itself by 10 mm. Fourteen thermocouples (K-type) with the diameters of 0.1 mm were attached on the outer surface of the capillary tube by welding. Fine thermocouple wires ensured fast response time, which is helpful for recording the time series of temperatures. The number of thermocouples was marked along the extended capillary tube in the clockwise direction. For instance, for the PHP with four turns (Fig. 1a), T3, T4, T8, T9, T12, and T13 were on the evaporation section, T2, T7, and T14 on the adiabatic section, T1, T5, T6, T10, and T11 on the condensation section, respectively. Thermocouples for PHPs with six and nine turns were marked in Fig. 1b and c. The fine K-type thermocouples (Omega) have the response time of 0.1 s, and the uncertainty of 0.1 °C after calibration.

It is difficult to measure temperatures inside the capillary tube. However, due to the thin wall thickness and high thermal conductivity of the copper capillary tube, temperature difference between outer and inner wall surface is very small. As an example, given a heating power of 60 W for the PHP with four turns, the outer and inner wall surface temperature difference was estimated only 0.04 °C, which is quite smaller than the temperature measurement uncertainty. Therefore, time series of outer wall surface temperatures could follow and represent the dynamic change of flow and heat transfer process inside the capillary tube.

The vacuum and charge procedures were performed using a special facility designed in our laboratory. The PHP was initially baked at 150 °C in an oven, evacuated to a pressure of 7.5×10^{-4} torr for 8 h. The PHP was then charged with the working fluid, and sealed. The final net liquid charged in the PHP was the weight difference before and after the PHP was charged with liquid. The weight measurement was carried out by an electronic balance with the accuracy of 0.01 g. Charge ratio is defined as the liquid volume to the total inside volume of the PHP. The charge ratio was estimated to have an uncertainty of 1%.

FC-72 and deionized, degassed water were used as the working fluids, with the former one having smaller saturation temperature, surface tension, and latent heat of evaporation than water, as seen from Table 1.

3. Chaotic analysis methods

3.1. Phase space reconstruction

The multidimensional phase space portraits can be reconstructed from the time series of temperature fluctuations [14]. The experimentally obtained time series signal, $T(t)$, is digitized with a time step of Δt, the resultant $(m+1)$ values of the signal, $T(i \cdot \Delta t)$ are stored for

$$i = 0, 1, 2 \ldots, m \tag{1}$$

The vector time series is defined as

$$\mathbf{X}(t) = [T(t), T(t+\tau), T(t+2\tau), \ldots T(t+(m-1)\tau)]^T \tag{2}$$

where m is the embedded dimension, τ is the time delay. The dynamic properties of systems could be studied by reconstruction of the phase space if $m \geqslant 2D+1$, where D is the fractal dimension of the system.

3.2. Phase portrait of strange attractors

An important chaotic analysis is the phase portrait, which can be performed by the stroboscope coordination [14]. Coordinates of attractor points are computed in terms of the subsequent samples between which the distance is the time delay τ. When τ is too small, the attractor gets flattened, making the further analysis of structure impossible. When τ is too large, the attractor becomes too complex, and further analysis gives wrong information about the dynamic behavior of the system. Thus, the selection of time delay is important in the analysis of the attractor properties. However, the selection of τ cannot be done automatically but should be checked after each computation manually [15]. Several methods such as the time-delay method, mutual information method, autocorrelation method, and complex autocorrelation method, could be used to decide suitable time delay for the attractor reconstruction [15]. In this study, the proper value of τ was decided using the complex autocorrelation method. Note that the suitable time delay that is finally determined for attractor reconstruction is different from run to run.

3.3. Correlation dimension

To compute the correlation dimension of the time series $T(t)$, their trajectories reconstructed by resorting to time embedding were used. From the trajectories of the vector time series, the correlation integral (the space correlation function) of the process, $C(r)$, is defined by Grassberger and Procaccia [16] as

$$C(r) = \lim_{N\to\infty} \times \frac{1}{N^2}\left[\text{number of pairs } (i,j) \text{ whose distance } |\mathbf{X}_i(t) - \mathbf{X}_j(t)| < r\right] \tag{3}$$

Usually,

$$C(r) = \lim_{N\to\infty} \frac{1}{N^2} \sum_{i=1}^{N} \sum_{j=1}^{N} H[r - |\mathbf{X}_i(t) - \mathbf{X}_j(t)|], \quad i \neq j \tag{4}$$

Table 1
Saturated thermophysical properties of different liquid coolants at 1 atm.

Fluid	T_{sat} (°C)	ρ_f (kg/m^3)	ρ_g (kg/m^3)	$C_{p,f}$ (J/kg K)	H_{fg} (kJ/kg)	σ (Nm)
FC-72	56.6	1600	13.43	1102	94.8	8.35×10^{-3}
Water	100	958	0.60	4217	2256.7	58.91×10^{-3}

where N is the number of data points, and H is the Heaviside function,

$$H[r-|\mathbf{X}_i(t)-\mathbf{X}_j(t)|]=\begin{cases}1 & \text{if } r>|\mathbf{X}_i(t)-\mathbf{X}_j(t)|\\ 0 & \text{otherwise}\end{cases} \tag{5}$$

The correlation integral, $C(r)$, was found to be a power function of r for small r as

$$C(r)=kr^{D_2} \tag{6}$$

where r is the radius of a hypersphere in the phase space. The slope of the plot of ln $C(r)$ versus ln$r$ is an estimate of the correlation dimension (D_2).

In this study, $C(r)$ was computed for an initial small embedded dimension m. The embedded dimension m is increased gradually and the correlation integral is re-estimated. Thus, a set of correlation dimensions is obtained. This process was stopped when the correlation dimension does not change anymore if the embedded dimension was further raised. Such a value was named as the correlation dimension D_2.

3.4. Kolmogorov entropy

The maximum-likelihood approach was used to estimate the Kolmogorov entropy [17]. In this algorithm, the entropy was determined from average number of steps required for a pair of vectors, which are initially within a specific distance l_c, to separate until the distance between the vectors becomes larger than l_c.

3.5. Rescaled range analysis: Hurst exponent

The rescaled range (R/S) analysis characterizes correlations in time series data with the Hurst exponent H [18]. When a positive correlation in time series data exists, the Hurst exponent, H, are between 0.5 and 1. Higher values of H indicate the stronger persistent trend. For uncorrelated data, i.e., stochastic data, H is about 0.5. When the value of H is in the range of 0–0.5, the data is negatively correlated, indicating the anti-persistency. From time series $T(t)$, the cumulative departure $B(t,u)$ to the average is computed in the range from $t+1$ to $t+\tau$:

$$B(t,u)=\sum_{u=1}^{t}T(u)-\langle T\rangle_\tau \tag{7}$$

where $\langle T\rangle_\tau$ is the average value of $T(t)$ over the subperiod τ. The sample sequential range $R(t,\tau)$, is defined as

$$R(t,\tau)=\max B(t,u)-\min B(t,u)\quad \text{for } 0\leqslant u\leqslant\tau \tag{8}$$

Then, the rescaled range $R(t,\tau)/S(t,\tau)$, is a power function of τ as follows, where $S(t,\tau)$ is the standard deviation calculated for subperiod τ:

$$\frac{R(t,\tau)}{S(t,\tau)}\propto\tau^H \tag{9}$$

The value of H can be evaluated from the slope of the logarithmic plot of $R(t,\tau)/S(t,\tau)$ as a function of τ.

4. Results and discussion

4.1. Traditional analysis of time series

In total, 148 experimental runs were performed. The operation parameters are as follows: working fluids of FC-72 or water, number of turns of 4, 6, and 9, charge ratios (α from 50% to 80%, inclination angles (θ from 5° (near horizontal) to 90° (vertical), heating power (Q) from 7.5 to 60.0 W. The range of heating power corresponds to the heat flux in terms of internal surface area (q) from 10.4 to 27.7 kW/m^2. Table 2 shows operating parameters for the runs that are involved in the present paper. The room environment temperature was fixed as 24 °C using the air conditioning system.

Table 2
Runs that are involved in the present paper.

Run number	Working fluid	Charging ratio (%)	Inclination angle (°)	Heating power (W)	Heat flux (W/m^2)	Turns
1	FC-72	50	5	15.0	10,393	4
11	FC-72	50	40	25.0	17,322	4
17	FC-72	50	90	40.0	27,715	4
22	FC-72	60	15	25.0	17,322	4
26	FC-72	60	40	25.0	17,322	4
29	FC-72	60	40	60.0	27,715	6
31	FC-72	60	90	25.0	10,393	4
33	FC-72	60	90	60.0	27,715	6
42	FC-72	70	5	15.0	10,393	4
46	FC-72	70	15	25.0	17,322	4
61	FC-72	70	40	60.0	27,715	6
68	FC-72	70	90	40.0	27,715	4
69	FC-72	70	90	40.0	12,317	9
78	FC-72	80	15	37.5	17,322	6
81	FC-72	80	40	25.0	17,322	4
87	Water	50	5	22.5	10,393	6
94	Water	50	90	37.5	17,322	6
96	Water	60	15	25.0	17,322	4
106	Water	60	90	25.0	17,322	4
110	Water	70	5	22.5	10,393	6
111	Water	70	15	15.0	10,393	4
112	Water	70	15	22.5	10,393	6
113	Water	70	15	25.0	17,322	4
115	Water	70	15	40.0	27,715	4
117	Water	70	40	15.0	10,393	4
119	Water	70	40	40.0	27,715	4
121	Water	70	90	25.0	17,322	4
123	Water	70	90	40.0	27,715	4
144	Water	80	40	60.0	27,715	6
146	Water	80	90	25.0	17,322	4

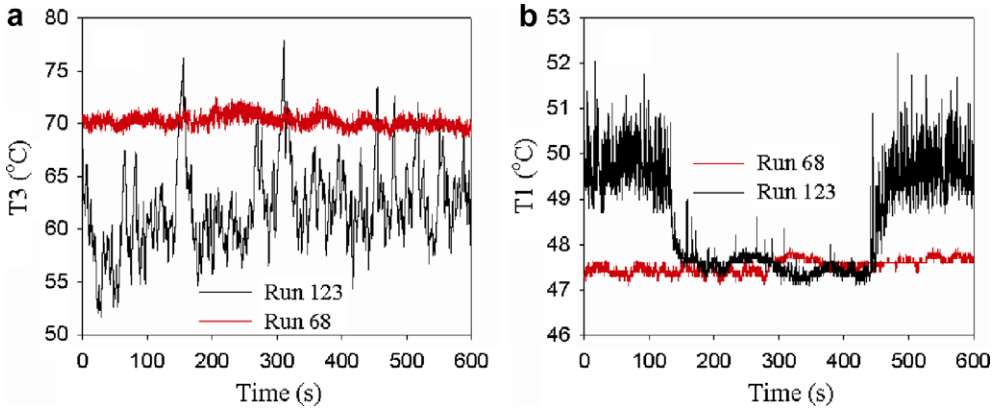

Fig. 2. Time series of temperatures for FC-72 and water PHPs, run 68 ($\alpha = 70$, $\theta = 90°$, $Q = 40.0$ W, four turns, FC-72 PHP), run 123 ($\alpha = 70$, $\theta = 90°$, $Q = 40.0$ W, four turns, water PHP).

For each run, the heating power was specified first. After the PHP system evolved the initial transition period, the time series of the 14 temperatures was recorded by the high speed data acquisition system. The initial waiting time was usually from 0.5 to 1 h.

Fig. 2a and b shows the time series of T3 on the evaporation section and T1 on the condensation section. It is seen that FC-72 PHP has small temperature oscillation both on the evaporation and condensation sections for run 68. However, water PHP has largest temperature oscillation on both sections for run 123. The time series of temperatures on the adiabatic section is similar to that on the condensation section for both FC-72 and water PHPs. This finding is consistent with our previous experimental results in Zhang et al. [19]. Here ΔT_{max} is defined as the temperature difference between the maximum and minimum values within ten minutes for PHPs. It is found that FC-72 PHPs only have the ΔT_{max} values in a couple of degrees. The largest ΔT_{max} approaches 3 °C for run 11. Water PHPs, however, have large temperature oscillation amplitudes with several tens of degrees. Previous visualizations show that water PHP may have short period with stationary fluid inside, during which the wall temperatures are continuously increased [13]. After such a short period, the sudden triggered fluid movement in the capillary tube significantly improves heat transfer, lowering the wall temperatures quickly. This is the reason why water PHPs have large temperature oscillation amplitudes. The instantaneous stationary fluid phenomenon does not exist in FC-72 PHPs due to the lower latent heat of evaporation of FC-72 than that of water [13].

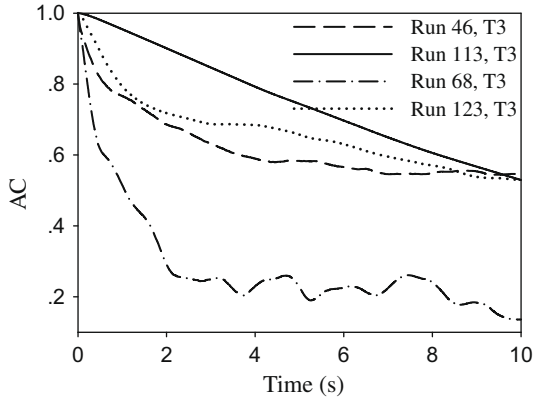

Fig. 3. Autocorrelation function of time series of T3, FC-72 PHPs: run 46 ($\alpha = 70$, $\theta = 15°$, $Q = 25.0$ W, four turns), run 68 ($\alpha = 70$, $\theta = 90°$, $Q = 40.0$ W, four turns), water PHPs: run 113 ($\alpha = 70$, $\theta = 15°$, $Q = 25.0$ W, four turns), run 123 ($\alpha = 50$, $\theta = 5°$, $Q = 15.0$ W, four turns).

Autocorrelation function (ACF) of the time series depicted in Fig. 3 are computed as

$$AC(\tau) = \frac{\sum_{i=1}^{N}(T_{i+\tau} - \langle T\rangle)(T_i - \langle T\rangle)}{\sum_{i=1}^{N}(T_i - \langle T\rangle)^2} \tag{10}$$

ACF helps to determine how quickly signals or process change with respect to time and whether a process has a periodic component. The autocorrelation function will have its largest value of $AC = 1$ at $\tau = 0$. As shown in Fig. 3, ACF is decreased with respect to time, indicating that prediction ability of the system is finite, which is the feature of the chaotic motion of PHPs. ACF is decreased much quickly for FC-72 PHPs than that for water PHPs, indicating less prediction ability of FC-72 PHPs than that of water PHPs.

4.2. The nonlinear analysis

Using the method described in Section 3.2, the attractor reconstructions were carried out. For the whole 148 runs, three typical attractor patterns were identified, as shown in Fig. 4. The type-I attractor shows the narrow and slim pattern, corresponding to low dimension chaotic properties of PHPs (Fig. 4a). Some water PHPs have such attractor patterns. The type-II attractor displays slight wider distribution than the type-I pattern in the phase space (Fig. 4b), corresponding to moderate chaotic properties of PHPs. It is seen from Fig. 4b that some parts of the attractor pattern are densely populated in the phase space, indicating that trajectory orbits are accumulated in such a local region. The local densely populated attractor pattern includes the information with both smaller positive and larger negative Lyapunov exponents of the system. For the run shown in Fig. 4b, the positive and negative Lyapunov exponents are 0.75 and −0.95, respectively. Self-resemble structure can be easily identified for the type-II attractor pattern.

Physical explanation of the self-resemble attractor pattern of the PHP system is given as follows. The PHP system is an open system. Heat is finally dissipated to the environment through the fin heat sink automatically without specific artificial intervention. When the heat flux is very small, the mixture of vapor plug and liquid slug is randomly populated in the capillary tube. If the heat flux is increased to a specific value, the PHP system begins to be far away from the equilibrium state. The local liquid temperature in the capillary tube is significantly higher than the saturation temperature corresponding to its pressure. Bubble nucleation and growth can take place at a specific location first, leading to the locally pressure rise which induces the bulk fluid circulation in the capillary tube.

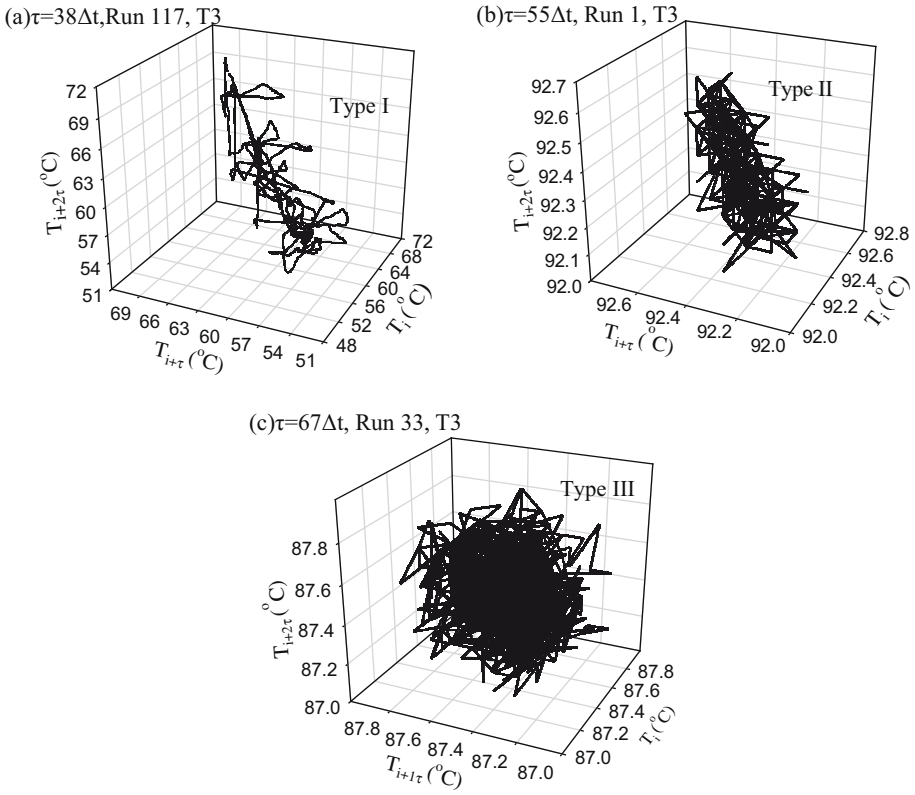

Fig. 4. Three types of attractor patterns, (a): type-I – low dimension chaotic PHP, run 117 ($\alpha = 70$, $\theta = 40°$, $Q = 15.0$ W, four turns, water PHP), (b): type-II – moderate dimension chaotic PHP, run 1 ($\alpha = 50$, $\theta = 5°$, $Q = 15.0$ W, four turns, FC-72 PHP), (c) type-III – high dimension chaotic PHP, run 33 ($\alpha = 60$, $\theta = 90°$, $Q = 60.0$ W, FC-72 PHP).

Meanwhile, the ordered pattern of vapor plugs and liquid slugs begins to occur from the initial randomly distributed mixture structure without heating. Because the temperature recordings at the wall surface follow the transient response of the mixture pattern inside the capillary tube, thus self-resemble attractor pattern appears. The bulk fluid circulation and related flow pattern in the glass capillary of PHP are reported in Xu et al. [13].

The type-III attractors have more scattered distribution in the phase space. This indicates high dimension chaotic properties of PHPs. Attractor pattern shown in Fig. 4 gives strong evidence that PHPs are deterministic chaotic systems, not periodic or random ones. This is because the strange attractor of a periodic system is an O-ring structure, and the attractor is populated everywhere in the phase space for a random system.

Fig. 5 shows the relationship between the correlation integral versus radius of hypersphere or the scale in phase space, based on the time series of temperature T3. Fig. 5a is for the FC-72 PHP with six turns (run 61: $\alpha = 70$, $\theta = 40°$, $Q = 60.0$ W). The suitable delay time τ is 10. It is observed that slopes of $\ln C(r)$ versus $\ln r$ are increased with increase in the embedded dimension m. However, curves of $\ln C(r) - \ln r$ become linear and parallel with each other when m is larger than 15. The curve slope is the correlation dimension, approaching the saturated value under such circumstance.

For the water PHP with six turns (run 112: $\alpha = 70$, $\theta = 15°$, $Q = 22.5$ W, see Fig. 5b), there are two linear sections corresponding to two correlation dimensions, indicating the multiscale phenomenon. Large slope of the curves $\ln C(r) - \ln r$ gives the high correlation dimension, referring to high frequency, small scale temperature oscillations, caused by miniature bubbles or short vapor plugs dynamically flowing in PHP channels. The lower correlation dimension corresponds to temperature oscillations with low frequency and large amplitude caused by elongated bubbles

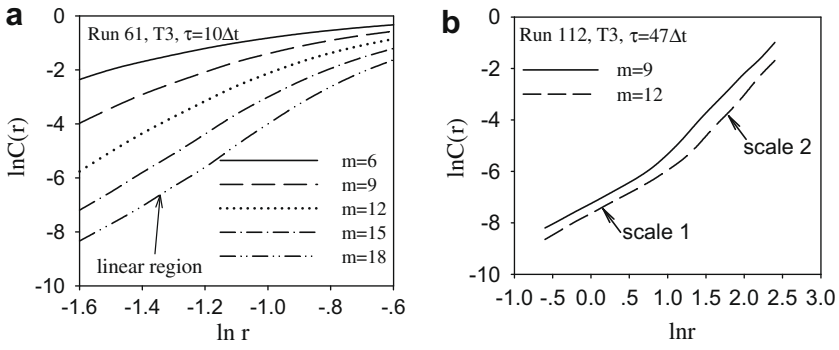

Fig. 5. Curves of $\ln C(r)$ versus $\ln r$, (a) FC-72 PHP, run 61 ($\alpha = 70$, $\theta = 40°$, $Q = 60.0$ W, six turns), (b) water PHP, run 112 ($\alpha = 70$, $\theta = 15°$, $Q = 22.5$ W, six turns).

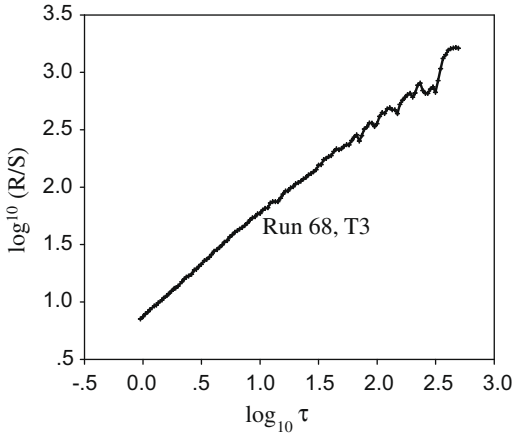

Fig. 6. $\log_{10}(R/S)$ versus $\ln\tau$ for run 68 (FC-72 PHP, $\alpha = 70$, $\theta = 90°$, $Q = 40.0$ W, four turns).

dynamically flowing in water PHPs. Multiscale phenomenon identified by the chaotic analysis in this study is similar to that observed in an evaporator with a vapor–liquid–solid boiling flow by Liu et al. [20]. The definitive physical interpretation on the multiscale correlation dimension remains to be further studied for water PHPs. It is noted that the multiscale phenomenon may not occur in all the chaotic systems. As indicated in this study, the multiscale phenomenon is not observed for FC-72 PHPs.

Fig. 6 gave the result of the rescaled range analysis based on time series of T3 for the FC-72 PHP with four turns (run 68: $\alpha = 70$, $\theta = 90°$, $Q = 40.0$ W). The perfect linear curve of $\log_{10}(R/S) - \log_{10}\tau$ reflects the self-resemble fractal behavior of the PHP system [14]. The slope of the curve is the Hurst exponent. The Hurst exponents were computed based on time series of T3, T4, T9, T12, T13 on the evaporation section for all the 148 runs. It is found that the Hurst exponents can have three subregions. The range from 0.75 to 0.85 of Hurst exponents covers about 20%. The Hurst exponent from 0.85 to 0.95 covers about 80%. The ultra-high Hurst exponent, i.e., from 0.95 to 0.98, covers very small percentage, i.e., less than 5%. High Hurst exponents of the PHP systems indicate very strong persistent behavior under the conditions examined here. Besides, high Hurst exponents indicate that the system is very sensitive to the initial conditions. Effect of a small external disturbance will last for a long time.

4.3. Effect of various parameters on the complexity of PHPs

Inclination angles, charge ratios, number of turns, working fluids, and heat fluxes are the typical parameters influencing the complexity degree of PHPs.

Consider effect of the inclination angles first. As noted by Zhang and Faghri [2], the PHP performance may or may not change with inclination angles. The dependence on orientation may be coupled with the number of turns. The previous and present experimental results show that the PHP performance is generally better in a vertical position ($\theta = 90°$, and some PHPs with only a few turns do not operate at horizontal orientation. It is observed that PHPs with four, six, and nine turns may not work at the exact horizontal position ($\theta = 0°$) in this study. However, they are working at slight inclination angles such as $\theta = 5°$. Correlation dimensions for FC-72 PHPs (runs 1 and 42) and water PHPs (runs 110 and 111) were shown in Fig. 7a, based on time series of T3, T4, T9, T12, and T13 on the evaporation section. The locations of these temperatures are shown in Fig. 1 for the three PHP units. The runs were selected for low inclination angles and small heating powers, which are difficult to activate the start-up process in this study. As can be seen from Fig. 7a, FC-72 PHPs have higher correlation dimensions than water PHPs, indicating easier start-up of FC-72 PHPs under the conditions considered. Another finding is that the complexity degrees are changed at different turns of PHPs, especially for the FC-72 PHPs. Left turns (see Fig. 1a) have lower correlation dimensions shown in Fig. 7a, corresponding to higher average temperatures on the left part of the evaporation section (see Fig. 7b). This phenomenon infers the bulk circulation flow during their start-up stage at low inclination angles and small heating powers. Because the aluminum fin heat sink has relative large capacity to dissipate heat on the condensation section, spatial variations of temperatures on the condensation section are very small for both PHPs.

Start-up process is an important issue for PHPs. The present study, incorporating the previous study by Xu and Zhang [21], identifies the easy start-up with the bottom heating mode than that with the top heating mode. This is similar to conventional heat pipes or loop heat pipes. Xu and Zhang [21] studied the start-up behavior of PHPs. Two types of start-up processes were identified depending on the heating power. After a small heating power is applied to the PHP, the wall temperature will be continuously increased to a high value. The fluid inside the capillary is absolutely stationary. This is the sensible heat receiving stage. Then the pulsating flow is suddenly triggered thus wall temperatures are sharply decreased followed by the steady oscillation stage. The temperature excursion, defined as the temperature difference between the maximum value achieved during the sensible heat receiving stage and the average value of the steady oscillation stage, can be up to 10 °C. However, if a high heating power is applied to the PHP, there is a smooth transition from the sensible heat receiving stage to the steady oscillation stage without the temperature excursion. Therefore, it is important to trigger the oscillating flow on time for the start-up of PHPs.

Correlation dimensions are used to quantify the complexity levels of the system, i.e., the number of independent variables to

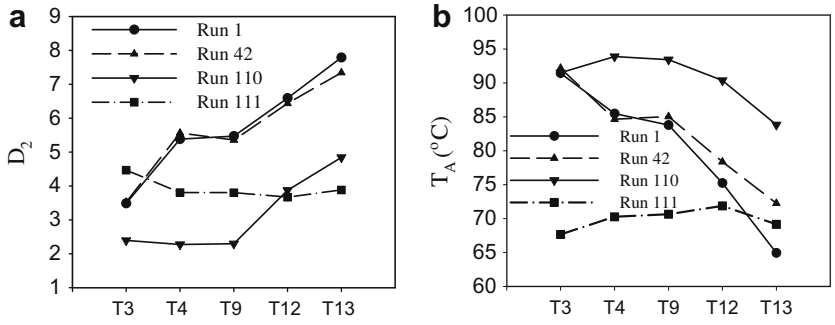

Fig. 7. Correlation dimension and its relationship with the average temperatures on the evaporation section, run 1 ($\alpha = 50$, $\theta = 5°$, $Q = 15.0$ W, four turns, FC-72 PHP), run 42 ($\alpha = 70$, $\theta = 5°$, $Q = 15.0$ W, four turns, FC-72 PHP), run 110 ($\alpha = 70$, $\theta = 5°$, $Q = 22.5$ W, six turns, water PHP), run 111 ($\alpha = 70$, $\theta = 15°$, $Q = 15.0$ W, four turns, water PHP).

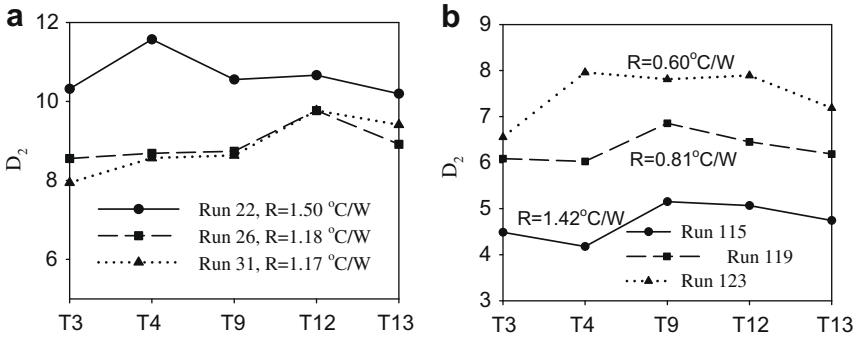

Fig. 8. Effect of inclination angles on the correlation dimension, (a) for FC-72 PHPs, (b) for water PHPs, operation parameters for selected runs are seen in Table 2.

describe the system. The higher the correlation dimensions, the more complex the system is. Variations of correlation dimensions and Kolmogorov entropies are not significant for different turns when inclination angles are greater than 10°. Correlation dimensions are higher for FC-72 PHPs than those for water PHPs, indicating more independent variables needed to describe the FC-72 PHPs. Correlation dimensions and Kolmogorov entropies are increased with increases in inclination angles for water PHPs, corresponding to the decreased thermal resistances (see Fig. 8b). For example, when the charge ratio is 0.7 and the heating power is 40 W, the thermal resistance is decreased from 1.42 °C/W at the inclination angle of 15° (run 115) to 0.61 °C/W at the inclination angle of 90° run 123). Here thermal resistance is defined as the temperature difference between the average temperature on the evaporation and condensation section, divided by the applied heating power.

However, the relationship between the chaotic parameters (correlation dimensions, Kolmogorov entropies) and the thermal resistance is different for FC-72 PHP and water PHP. As shown in Fig. 8a, the FC-72 PHP with high correlation dimensions for the run 22 also has large thermal resistance of 1.50 °C/W at $\theta = 15°$. Alternatively, the other two runs of 26 and 31 with lower correlation dimensions have lower thermal resistances of 1.17–1.18 °C/W at θ of 40° and 90°. It is observed that the chaotic parameters and thermal resistances are more sensitive to inclination angles for water PHPs than those for FC-72 PHPs. FC-72 has lower latent heat of evaporation than water. Much vapor can be evaporated from liquid for FC-72 than that for water when both receive the same heat, causing higher chaotic level for FC-72 PHPs. Therefore, effect of the inclination angle on the complexity levels and thermal performance is decreased for FC-72 PHPs.

Effect of the charge ratios is considered here. If the charge ratio is too low, a small amount of inside volume of the PHP is occupied by liquid. Dry-out on the evaporation section takes place easily. If the charge ratio is too high, there are not enough bubbles to pump the fluid movement in PHPs. Zhang and Faghri [2] recommended a wide range of charge ratios from 20% to 80%. This is because the optimal value of charge ratio depends on many factors such as PHP geometry and structure, number of turns, working fluids, fin heat sink design, etc. In this study, the optimal charge ratio is from 60% to 80%, which is consistent with that for PHPs with three turns and working fluids of FC-72 and water in Zhang et al. [19].

Fig. 9a shows correlation dimensions for FC-72 PHPs with three charge ratios of 50% (run 11), 60% (run 26), and 80% (run 81) with $\theta = 40°$, $Q = 25$ W, and number of turns of 4. Correlation dimensions are larger than 7 around the optimal charge ratio. They are slight larger for the charge ratio of 60%, corresponding to slight lower thermal resistance of 1.15 °C/W. The other two charge ratios of 50% and 80% have slight larger thermal resistances.

Fig. 9b illustrates correlation dimensions based on the time series of temperatures on the evaporation section with charge ratios from 60% (run 106) to 80% (run 146) for water PHPs. Better thermal performance was achieved with lower thermal resistance of 0.95 °C/W at the charge ratio of 70%, relating to apparently higher correlation dimensions at such a charge ratio.

5. Conclusions

The time series of temperatures on the evaporation, adiabatic, and condensation sections of PHPs were recorded. Experiments were performed over wide parameter ranges. New conclusions are summarized as follows:

- Pulsating heat pipes are deterministic chaotic systems, not periodic or random systems.
- Autocorrelation function coefficients for both FC-72 and water PHPs are decreased with respect to time, indicating that the prediction ability of the system is finite.

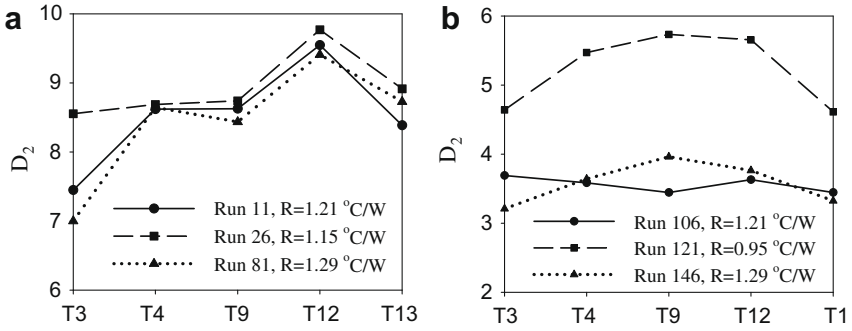

Fig. 9. Effect of charge ratios on the correlation dimension, (a) for FC-72 PHPs, (b) for water PHPs, operation parameters for selected runs are seen in Table 2.

- Three typical attractor patterns were identified. The type-I attractors have slim distribution, type-II attractors have wider distribution with self-resemble structure, type-III attractors have scatter distribution, in the phase space.
- PHPs have high Hurst exponents in the range from 0.85 to 0.95, indicating very strong persistent property which ensures stable oscillation in a long time span.
- Water PHPs have low frequency, large amplitude, and high frequency, small amplitude oscillations, leading to two linear sections in the curve of $\ln C(r)$ versus $\ln r$, indicating the multiscale phenomenon. But the multiscale phenomenon was not observed for FC-72 PHPs.
- At low inclination angles ($\theta = 5^\circ$), correlation dimensions are not uniform at different turns, indicating the bulk circulation flow, especially for FC-72 PHPs. The non-uniformity behavior disappears for $\theta > 10$–15°. Correlation dimensions and Kolmogorov entropies are increased with increases in inclination angles for water PHPs, corresponding to the decreased thermal resistances. Alternatively, the correlation dimensions are higher at smaller inclination angles ($\theta = 15^\circ$) for FC-72 PHPs, corresponding to poorer thermal performance.
- The optimal charge ratios are about 60–70% for both FC-72 and water PHPs with four, six, and nine turns. PHPs have better thermal performance at such a narrow range of charge ratio.
- FC-72 PHPs have complex relationship between correlation dimensions and number of turns. Correlation dimensions are increased with increases in the number of turns for water PHPs.
- Both FC-72 and water PHPs have higher correlation dimensions when the heat flux is increased.

Acknowledgements

This work is supported by the National Science Fund for Distinguished Young Scholars from the National Natural Science Foundation of China (No. 50825603) and the Natural Science Foundation of China (No. 50776089).

References

[1] H. Akachi, F. Polasek, P. Stulc, Pulsating heat pipes, in: Proceedings of the Fifth International Heat Pipe Symposium, Melbourne, Austria, 1996, pp. 208–217.
[2] Y. Zhang, A. Faghri, Advances and unsolved issues in pulsating heat pipes, Heat Transfer Eng. 29 (2008) 20–44.
[3] S. Maezawa, K. Gi, A. Minamisawa, H. Akachi, Thermal performance of capillary tube thermosyphon, in: Proceedings of the IX International Heat Pipe Conference, Albuquerque, New Mexico, 1996, pp. 791–795.
[4] Y. Zhang, A. Faghri, Heat transfer in a pulsating heat pipe with open end, Int. J. Heat Mass Transfer 45 (2002) 755–764.
[5] B. Holley, A. Faghri, Analysis of pulsating heat pipe with capillary wick and varying channel diameter, Int. J. Heat Mass Transfer 48 (2005) 2635–2651.
[6] S. Khandekar, M. Schneider, P. Schafer, R. Kulenovic, M. Groll, Thermofluid dynamics study of flat plate closed loop pulsating heat pipes, Microscale Thermophys. Eng. 6 (2002) 303–318.
[7] S. Khandekar, P. Charoensawan, M. Groll, P. Terdtoon, Closed loop pulsating heat pipes part B: visualization and semi-empirical modeling, Appl. Therm. Eng. 23 (2003) 2021–2033.
[8] R.T. Dobson, Theoretical and experimental modeling of an open oscillatory heat pipe inducing gravity, Int. J. Therm. Sci. 43 (2004) 113–119.
[9] B.Y. Tong, T.N. Wong, K.T. Ooi, Closed loop pulsating heat pipe, Appl. Therm. Eng. 21 (2001) 1845–1862.
[10] L. Lin, R. Ponnappan, J. Leland, Experimental investigation of oscillating heat pipes, AIAA J. Thermophys. Heat Transfer 15 (2001) 395–400.
[11] Q. Cai, C.L. Chen, J.F. Asfia, Operating characteristic investigations in pulsating heat pipes, ASME J. Heat Transfer 128 (2006) 1329–1334.
[12] H.B. Ma, C. Wilson, Q. Yu, U.S. Choi, M. Tirumala, An experimental investigation of heat transport capability in a nanofluid oscillating heat pipe, ASME J. Heat Transfer 128 (2006) 1213–1216.
[13] J.L. Xu, Y.X. Li, T.N. Wong, High speed flow visualization of a closed loop pulsating heat pipe, Int. J. Heat Mass Transfer 48 (2005) 3338–3351.
[14] H.G. Schuster, Deterministic Chaos: An Introduction, Physik-Verlag Gmbh, Weinheim, 1984.
[15] R. Mosdorf, P. Cheng, H.Y. Wu, M. Shoji, Non-linear analysis of flow boiling in microchannels, Int. J. Heat Mass Transfer 48 (2005) 4667–4683.
[16] P. Grassberger, I. Procaccia, Measuring the strangeness of strange attractors, Physica D 9 (1983) 189–194.
[17] J.C. Schouten, F. Taken, C.M. van den Bleek, Maximum-likelihood estimation of the entropy of an attractor, Phys. Rev. E 49 (1994) 126–129.
[18] W. Chen, T. Hasegawa, A. Tsutsumi, K. Otawara, Y. Shigaki, Generalized dynamic modeling of local heat transfer in bubble columns, Chem. Eng. J. 96 (2003) 37–44.
[19] X.M. Zhang, J.L. Xu, Z.Q. Zhou, Experimental study of pulsating heat pipe using FC-72 ethanol and water as working fluids, Exp. Heat Transfer 17 (2004) 47–67.
[20] M.Y. Liu, A.H. Qiang, B.F. Sun, Chaotic characteristics in an evaporator with a vapor–liquid–solid boiling flow, Chem. Eng. Process. 45 (2006) 73–78.
[21] J.L. Xu, X.M. Zhang, Start-up and steady thermal oscillation of a pulsating heat pipe, Heat Mass Transfer 41 (2005) 685–694.